Discrete-vortex analysis of high Reynolds number flow past a rotating cylinder

Cite as: AIP Advances 10, 055104 (2020); doi: 10.1063/5.0004851
Submitted: 14 February 2020 • Accepted: 3 April 2020 •
Published Online: 4 May 2020

Wei Chen,[1,a] Chang-Kyu Rheem,[2,b] Yuanzhou Zheng,[3,4,c] Atilla Incecik,[5,d] Yongshui Lin,[1,a] and Zhixiong Li[6,e]

AFFILIATIONS

[1]School of Science, Wuhan University of Technology, Wuhan 430070, China
[2]Department of Ocean Technology, Policy and Environment, The University of Tokyo, Tokyo 1538505, Japan
[3]School of Navigation, Wuhan University of Technology, 430070 Wuhan, China
[4]Hubei Key Laboratory of Inland Shipping Technology, Wuhan 430070, China
[5]Department of Naval Architecture, Ocean and Marine Engineering, University of Strathclyde, Glasgow, Scotland G1 1XQ, United Kingdom
[6]School of Mechanical, Materials, Mechatronic and Biomedical Engineering, University of Wollongong, Wollongong, NSW 2522, Australia

[a]**Electronic addresses:** whutcw01@whut.edu.cn and linyongshui1226@whut.edu.cn
[b]**Email:** rheem@iis.u-tokyo.ac.jp
[c]**Author to whom correspondence should be addressed:** yzzheng@whut.edu.cn
[d]**Email:** atilla.incecik@strath.ac.uk
[e]**Email:** zhixiong_li@uow.edu.au

ABSTRACT

Flow past a rotating cylinder is investigated using a two-dimensional discrete vortex simulation method in this study. The simplified Navier–Stokes equation is solved based on the relationship between the surface pressure gradient and the generated surface vortex strength. The Reynolds number based on the cylinder diameter and flow velocity is 10^5. The non-dimensional rotation rate, α (the ratio of the cylinder surface velocity and flow velocity), is varied between 0 and 19, and four different wake formations (vortex shedding, weak vortex shedding, wake, and rotating wake formations) have been derived by the imposed rotation. The relationship between the hydrodynamics and wake formation is illustrated. Under vortex shedding and weak vortex shedding formations, periodical hydrodynamics is induced. Under wake formation, no gap between the positive-vorticity and negative-vorticity layers results in the steady hydrodynamics. The separation of the rotating wake induces the huge fluctuation of hydrodynamics under rotating wake formation. These are significant for a flow control technique and for the design of ocean and civil engineering structures. With the increasing rotation rate, the variation of mean hydrodynamics has been discussed and the maximum mean hydrodynamics is considered to be decided by the rotation rate. According to these wake formations, the vortex shedding, weak vortex shedding, wake, and rotating wake areas are identified. Combining the initial, increasing, and equivalent areas for mean hydrodynamics, two different area-divisions have been conducted for mean hydrodynamics and the relationship between the two area-divisions has been illustrated. Finally, the disappearance of vortex shedding and variation of the Strouhal number have been discussed in detail. The critical value for the disappearance of vortex shedding is $\alpha \approx 3.5$, and the Strouhal number remains steady initially and then decreases.

NOMENCLATURE

AS	aspect ratio
$C_d, \overline{C_d}$	drag coefficient and mean drag coefficient
$C_l, \overline{C_l}$	lift coefficient and mean lift coefficient
D, r	diameter and radius of the cylinder (m)
$ds, \Delta s_n$	length of surface vorticity at points s and n (m)
$dt, \Delta t$	time step (s)

f_v	vortex shedding frequency
F_x, F_y	force in the x and y direction (N)
M	mesh number of the surface
p, P_1, P_m	surface pressure gradient, mean pressure at point 1, and mean pressure at point m
q	surface velocity
Q_i, P_i	random numbers
Re, St	Reynolds number and Strouhal number
t, T	time (s) and non-dimensional time
U, U_τ	flow velocity and tangential velocity of the body surface (m/s)
U_∞, V_∞	flow velocity in the horizontal and vertical direction (m/s)
U_{mj}, V_{mj}	induced velocity at point m by vorticity at point j (m/s)
v_s	tangential velocity (m/s)
x_m, x_n, x_j	x coordinate of points m, n, and j (m)
y_m, y_n, y_j	y coordinate of points m, n, and j (m)

Greek symbols

α	rotation rate
β_m, β_n	tangential angle at point m and point n (rad)
$\gamma(s)$	strength of surface vorticity at point s (m/s)
$d\gamma(s)$	generated net vorticity in time dt at point s (m/s)
Δr_i	wake vortex diffusion radius
$\Delta\Gamma$, $\Delta\Gamma_j$	circulation of the vortex and circulation of the free vortex j
ρ, υ	density (kg/m^3) and kinematic viscosity (m^2/s)
w	rotating angular velocity (rad/s)

I. INTRODUCTION

Investigations of flow past a rotating cylinder have been conducted by many researchers through the theoretical, numerical, and experimental methods. Flow past a rotating cylinder is significant for hydrodynamics and for the design of ocean and civil engineering structures, such as the drilling pipes. In particular, flow of a rotating cylinder has been extensively applied for the flow control. An early laboratory experiment of Tokumaru and Dimotakis (1993) showed how the wake can be controlled by subjecting the cylinder to rotatory oscillations. The symmetric wake is broken, and drag reduction has been realized. Besides this, a significant increase in mean lift has been achieved by Modi (1997) through controlling flow past airfoils.

The hydrodynamic forces generated by a rotating cylinder in flow have been investigated by many researchers. Prandtl (1925) was one of the earliest researchers whose experimental results suggested that the maximum mean lift generated by a rotating cylinder in flow is 4π, which is called "Prandtl's limit" [Fig. 1(a)]. Then, the arguments that whether Prandtl's limit could be exceeded started. Tokumaru and Dimotakis (1993) reported that Prandtl's limit could be exceeded by using a method based on an inviscid point-vortex method, where the maximum mean lift coefficient is 20% larger than that limit. Chew *et al.* (1995) agreed with Prandtl's limit, and a maximum mean lift coefficient of 9.1 for $\alpha = 6$ at Re = 1000 was predicted. The results of Mittal and Kumar (2003) indicated that the mean lift at $\alpha = 5$ reached 27, which is much larger than Prandtl's limit. Bourguet and Lo Jacono (2014) investigated the mean lift of a rotating cylinder at Re = 100 based on two- and three-dimensional numerical simulation methods for $0 < \alpha < 4$, and their results indicated that the mean lift could reach 17 at $\alpha = 4$, which similarly exceeded 4π.

As shown in Fig. 1(a), the turbulent flow past a rotating cylinder at a supercritical Reynolds number ($Re \geq 3.0 \times 10^5$) was investigated by Karabelas *et al.* (2012), and the results showed that the mean lift was much smaller than that of Prandtl; even for $\alpha = 8$, the mean lift was only approximately 5.5 due to the turbulent flow. However, the laminar flow at low Reynolds numbers ($Re \leq 300$) of a rotating cylinder was investigated by Stojkovic *et al.* (2002), and their results indicated that Prandtl's limit could be greatly exceeded, with the increasing rotation rate; the trend for the mean lift is approximately the same as those of Mittal and Kumar (2003) and Bourguet and Lo Jacono (2014) with low Reynolds numbers. In particular, for

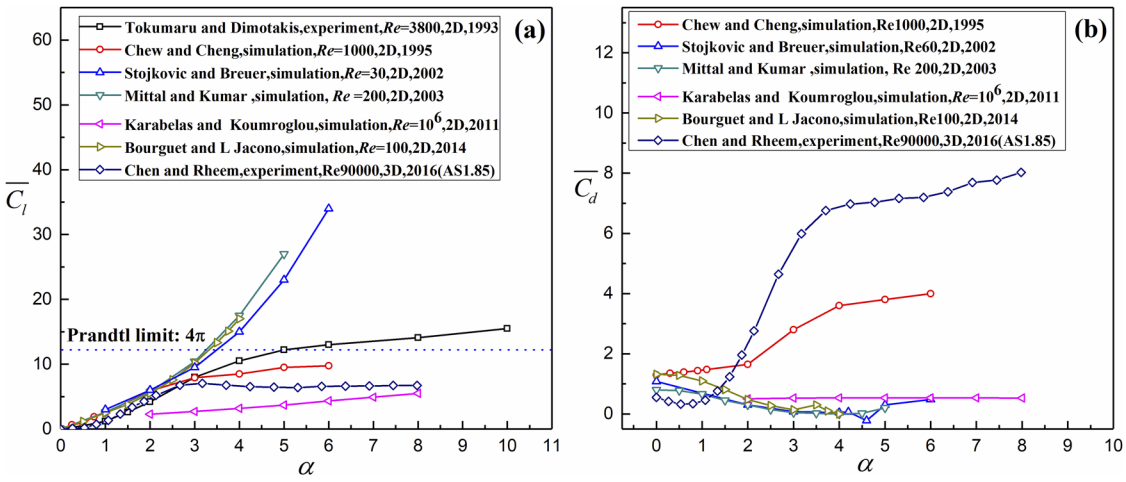

FIG. 1. (a) Mean lift coefficient, $\overline{C_l}$, and (b) mean drag coefficient, $\overline{C_d}$, vs rotation rate, α, from previous works (2D = two-dimensional).

the turbulent flow at the subcritical Reynolds number ($300 \le Re \le 3.0 \times 10^5$), Chen and Rheem (2019) conducted an experiment with rotating cylinders in flow, where the mean lift increased and then remained steady with increasing rotation rate, which is similar to those results of Chew *et al.* (1995) at the Reynolds number of 1000 and Tokumaru and Dimotakis (1993) at the Reynolds number of 3800.

The mean drag of previous researchers vs the rotation rate is shown in Fig. 1(b), and the variations in mean drag vs the rotation rate differ. At low Reynolds numbers, most of the researchers (Stojkovic *et al.*, 2002; Mittal and Kumar, 2003; and Bourguet and Lo Jacono, 2014) found that the mean drag would decrease with increasing rotation rate, and arguments that whether negative values of the mean drag would appear at $4 \le \alpha \le 6$ still remain. At the supercritical Reynolds number, Karabelas *et al.* (2012) suggested that the mean drag remains steady with the increase in rotation rate at $Re = 10^6$. At the subcritical Reynolds number, Chew *et al.* (1995) concluded that, with the increase in rotation rate, the mean drag increased and then remained steady at $Re = 1000$. Nevertheless, the mean drag of Chen and Rheem (2019) initially decreases to nearly zero, but without negative values, then dramatically increases, and finally remains steady. The increasing and steady components are found to be similar to those in the results of Chew *et al.* (1995).

Except for the hydrodynamics, the wake formation as a significant component of a rotating cylinder in flow has been investigated at different Reynolds numbers (Fujisawa *et al.*, 1991; Chew *et al.*, 1995; Shiels and Leonard, 2001; Mittal and Kumar, 2003; Mittal, 2004; Kumar *et al.*, 2011a; Du and Dalton, 2013; Rao *et al.*, 2013; Bourguet and Lo Jacono, 2014; Rao *et al.*, 2015; Sun *et al.*, 2016; Schulmeister *et al.*, 2017; Munir *et al.*, 2018; Palkin *et al.*, 2018; and Hadžiabdić *et al.*, 2019). Among these, the critical value of vortex shedding cease is attracting a few researchers (Diaz *et al.*, 1983; Coutanceau and Menard, 1985; Chew *et al.*, 1995; Degani *et al.*, 1998; Mittal and Kumar, 2003; and Chen and Rheem, 2019).

The Reynolds numbers for ocean and civil engineering structures are usually located in the range of subcritical Reynolds numbers ($300 \le Re \le 3.0 \times 10^5$), where the laminar boundary layer of the structural surface has to undergo turbulent transition and the wake is narrower and disorganized, and the fluid-induced vibrations cause fatigue damage and even failure of these structures, which decreases the service life of these structures (Bearman, 1984; Williamson and Roshko, 1988; Blevins, 1990; and Yamamoto *et al.*, 2004). With imposed rotation, the vibrations still occur. Some works have been conducted for the flow past a rotating cylinder. However, the works of flow past a rotating cylinder with a wide range of rotation rates are poor, which are concluded in Fig. 1 (Tokumaru and Dimotakis, 1993; Chew *et al.*, 1995; and Chen and Rheem, 2019), in some of which the investigations of the mean drag are ignored. In addition, the intrinsic relationship of the hydrodynamics and wake formation has not been thoroughly illustrated. The rotation rates of previous studies are limited with a maximum of 8, and the possible consequences of the wake formation at a higher rotation rate are perplexed. The disappearance of vortex shedding and variation of the Strouhal number need to be clarified. These issues are addressed in the present work.

The present work is an attempt to resolve these issues of the flow past a rotating cylinder by a discrete vortex method (DVM), which has been verified to be adaptive for the high Reynolds number turbulent flow past a circular cylinder in previous works (Kimura and Tsutahara, 1987; Koumoutsakos and Leonard, 1995; Honoréwalther and Larsen, 1997; and Mustto *et al.*, 1998). Illustrating the hydrodynamics and wake formation with increasing rotation rate is significant for the design of ocean and civil engineering structures and for the flow control technique. In the present work, the Reynolds number is 10^5. The range of rotation rates from 0 to 19 is considered, which is wider than those in the open literature. The basic theory and the numerical simulation method are introduced in Sec. II. The results and discussion are presented in Sec. III. The conclusions of the present work are summarized in Sec. IV.

II. THE DVM CALCULATION METHOD

A discrete vortex method (DVM) has been introduced for the simulation of a rotating cylinder in flow. Differing from the DNS, RANS, and LES methods (Evangelinos *et al.*, 2000; Korpus *et al.*, 2000; and Al-Jamal and Dalton, 2004), the continuous vortex in flow is treated as a series of discrete point vortices and the Lagrange method is applied to trace the moving of point vortices.

A. The incompressible equation

The flow is assumed to be a two-dimensional, incompressible viscous fluid, which is governed by the Navier–Stokes equation as follows (Lewis, 2005):

$$\underset{(a)\ldots\ldots(b)\ldots\ldots\ldots(c)\ldots\ldots(d)}{\frac{\partial q}{\partial t} + q \cdot \nabla q = -\frac{\nabla p}{\rho} + \upsilon \nabla^2 q.} \tag{1}$$

Reading from left to right, unsteady (a) and convective fluid (b) motions are related to pressure gradients (c) and viscous shear stresses (d). In the discrete vortex method, term (b) is determined by the convection of all shedding vortex elements and term (d) is based on the viscous diffusion of all shedding vortex elements in the calculation area, at every time interval dt; after convection and diffusion, the Navier–Stokes equation can be simplified to the following form:

$$\frac{\partial q}{\partial t} = -\frac{\nabla p}{\rho}. \tag{2}$$

This equation expresses the relationship of the surface velocity q and surface pressure gradient p.

B. Vorticity convection and production in the shear layer

Vorticity is continuously created in the shear layer and shed into the flow, considering $d\gamma(s)$ as the net vorticity per unit length generated at point s in time dt; then, as shown in Fig. 2, the net vorticity flux leaving the control volume $abcd$ can be related to $d\gamma(s)$ (Lewis, 2005).

The equation is as follows:

$$d\gamma(s) \cdot ds = \left(\frac{1}{2}(v_s + dv_s)(\gamma(s) + d\gamma(s)) - \frac{1}{2}v_s\gamma(s)\right) \cdot dt. \tag{3}$$

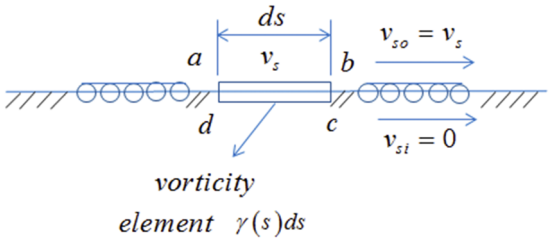

FIG. 2. Surface vorticity equivalent, where *vorticity* is created by the net vorticity flux in time *dt* in the cross *abcd*.

Neglecting the second-order products of infinitesimal quantities, the equation can then be shortened as follows:

$$\frac{d\gamma(s)}{dt} = \frac{d}{ds}\left(\frac{v_s^2}{2}\right). \tag{4}$$

The second term (right-hand side) is related to the pressure (based on the potential theory) as follows:

$$\frac{d}{ds}\left(\frac{v_s^2}{2}\right) = -\frac{1}{\rho}\frac{dp}{ds}. \tag{5}$$

Finally, the relationship is as follows:

$$\frac{d\gamma(s)}{dt} = \frac{d}{ds}\left(\frac{v_s^2}{2}\right) = -\frac{1}{\rho}\frac{dp}{ds}. \tag{6}$$

Here, the relationship between the generated vortex strength at *dt* and the surface pressure gradient can be constructed.

Taking the rotation into consideration, Eq. (3) can be expressed as follows:

$$d\gamma(s)\cdot ds = \left(\left(\frac{1}{2}(v_s + dv_s) + wr\right)(\gamma(s) + d\gamma(s))\right. \\ \left. -\left(\frac{1}{2}v_s + wr\right)\gamma(s)\right)\cdot dt. \tag{7}$$

Finally, the expression can be presented as follows:

$$\frac{d\gamma(s)}{dt} = \frac{d}{ds}\left(\frac{(v_s + wr)^2}{2}\right) = -\frac{1}{\rho}\frac{dp}{ds}. \tag{8}$$

Compared to the non-rotating condition, the rotation of the cylinder accelerates the net vorticity flux in time *dt* and changes the surface pressure gradient.

C. Boundary condition and conservation theory

For a two-dimensional body in viscous flow, the surface vortex element is generated on the body surface of the cylinder model, as shown in Fig. 3, and the no-slip condition of generated surface vorticity can be described as

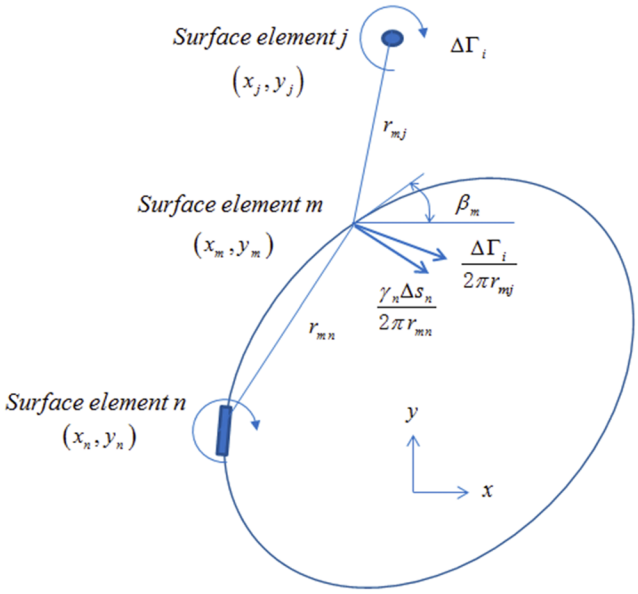

FIG. 3. Discrete surface vorticity model for a two-dimensional body.

$$U_\tau = \sum_{n=1}^{M} K(s_m, s_n)\gamma(s_n) + U_\infty \cos\beta_m + V_\infty \sin\beta_m \\ + \sum_{j=1}^{Z} \Delta\Gamma(U_{mj}\cos\beta_m + V_{mj}\sin\beta_m) = 0. \tag{9}$$

For a rotating cylinder model, the equation will be

$$U_\tau = \sum_{n=1}^{M} K(s_{m\_r}, s_{n\_r})\gamma(s_{n\_r}) + \frac{\Gamma}{2\pi r} + U_\infty \cos\beta_{m\_r} + V_\infty \sin\beta_{m\_r} \\ + \sum_{j=1}^{Z} \Delta\Gamma(U_{mj\_r}\cos\beta_{m\_r} + V_{mj\_r}\sin\beta_{m\_r}) = wR, \tag{10}$$

where

$$K(s_m, s_n) = \begin{cases} = -0.5 & (\text{if } s_m = s_n) \\ = \frac{\Delta s_n}{2\pi}\left(\frac{(x_m - x_n)\sin\beta_n - (y_m - y_n)\cos\beta_n}{(y_m - y_n)^2 + (x_m - x_n)^2}\right) & (\text{else}), \end{cases} \tag{11}$$

$$U_{mj} = \frac{1}{2\pi}\frac{y_m - y_j}{(y_m - y_j)^2 + (x_m - x_j)^2}, \tag{12}$$

$$V_{mj} = -\frac{1}{2\pi}\frac{x_m - x_j}{(y_m - y_j)^2 + (x_m - x_j)^2}. \tag{13}$$

The boundary conditions of the cylinder model and the rotating cylinder model are different, as the relationship $\Gamma/(2\pi r) \approx wR$ can be obtained, which indicates that the equations of boundary conditions for the cylinder model and rotating cylinder model are approximately the same, but for the rotating cylinder model, the wake vortices are dramatically affected by rotation and inclined into the rotation direction.

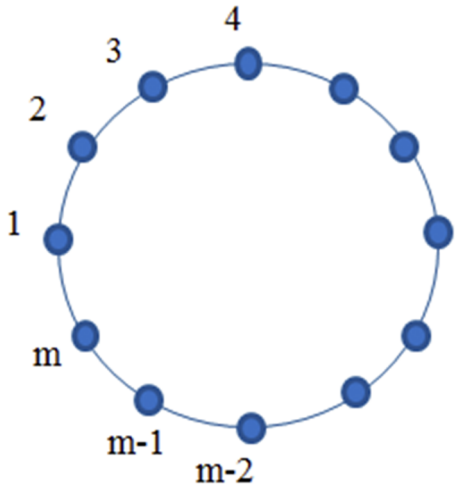

FIG. 4. Division of the elements on the body surface.

During the calculation, all vorticity in the calculation area at every moment should follow the circulation conservation of Kelvin's theorem,

$$\sum_{n=1}^{M} \gamma(s_n)\Delta s_n + \sum_{j=1}^{Z} \Delta\Gamma_j = 0. \tag{14}$$

D. Vorticity diffusion

At time dt, convection of generated surface vortex elements is shown in Fig. 3, and for the surface vortex element, convection components are from wake vorticity and surface vorticity, considering the viscosity of the flow; diffusion over a series of time steps can be expressed as follows:

$$x_i' = x_i + \Delta r_i \cos\Delta\theta_i, \tag{15}$$

$$y_i' = y_i + \Delta r_i \sin\Delta\theta_i, \tag{16}$$

where

$$\Delta\theta_i = 2\pi Q_i,\ \Delta r_i = \{4v\cdot\Delta t\cdot\ln(1/P_i)\}^{1/2}. \tag{17}$$

E. Calculation of pressure and force coefficients

After convection and diffusion calculation in the calculation domain, as shown in Fig. 4, surface pressure at point m on the body surface can be expressed as follows:

$$P_m = P_1 - \frac{\rho}{dt}\sum_{n=1}^{M}\gamma(s_n)\Delta s_n. \tag{18}$$

Finally, the drag and lift coefficients are defined as follows:

$$C_d = \frac{F_x}{\frac{1}{2}\rho DU^2}, \tag{19}$$

$$C_l = \frac{F_y}{\frac{1}{2}\rho DU^2}. \tag{20}$$

F. Numerical method applicability and effectiveness

For the DVM, the displacement of the flow in one-time step should be smaller than the length of the single surface vorticity, and the expression of the time step is as follows:

$$\Delta t = k\frac{\pi D}{MU}, \tag{21}$$

where k is smaller than 1.0 and the value of 0.5 is selected, which indicates that, in the time step, the displacement of the flow equals to half length of the single surface vorticity.

As indicated in Eq. (21), the time step is concerned with the surface element number. In order to select a suitable surface element number, the rigid mounted cylinder model is constructed. The mean drag coefficients under different Reynolds numbers and surface element numbers are shown in Fig. 5(a). Compared with those of Lamb (1993) and Schlichting and Gersten (2016), the resistance loss phenomenon due to turbulent flow at Re ≈ 10^6 is missed in the present results. At $10^3 \le$ Re $\le 2.0\times10^5$, the mean drag

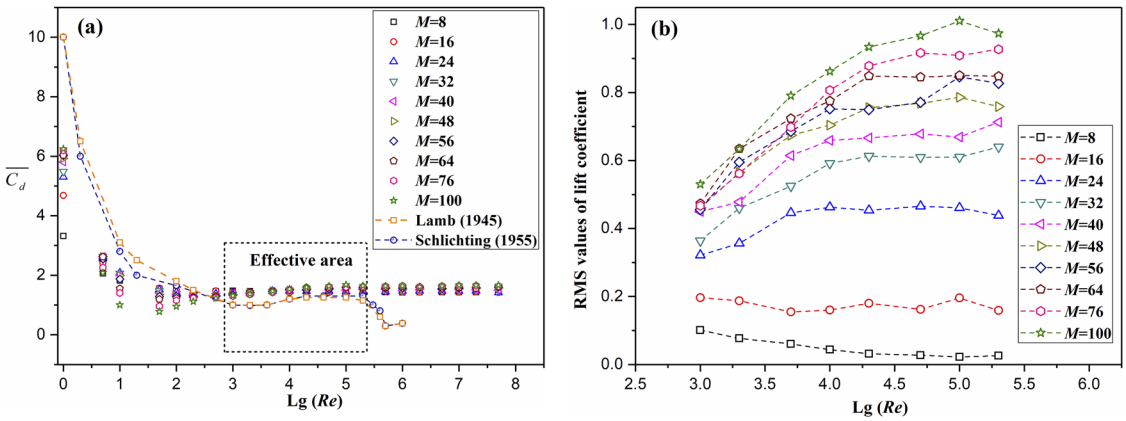

FIG. 5. (a) The mean drag coefficients under different Reynolds numbers and (b) the rms values of the lift coefficient in the effective area.

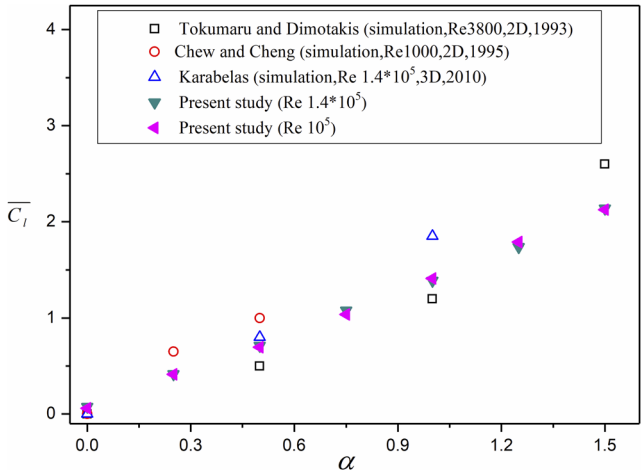

FIG. 6. The mean lift coefficients vs rotation rate.

coefficients are steady and close to those of Lamb (1993) and Schlichting and Gersten (2016), which indicates that the present discrete vortex method is effective at $10^3 \le Re \le 2.0 \times 10^5$ (in $300 \le Re \le 3.0 \times 10^5$). The rms (root mean square) values of the lift coefficient at $10^3 \le Re \le 2.0 \times 10^5$ are shown in Fig. 5(b), and the rms values increase with the increasing surface element number and are close to each other at $M \ge 48$, which indicates that the results for these element numbers are more reliable. Taking the calculation time into consideration, $M = 48$ is selected for the following numerical calculation.

Figure 6 shows the mean lift coefficient under different rotation rates, and the values of the mean lift increase with increasing rotation rate. The mean lift coefficient of the present study is close to that of Tokumaru and Dimotakis (1993), Chew *et al.* (1995), and Karabelas *et al.* (2012) at subcritical Reynolds numbers. All of these indicate that the present discrete vortex method is applicable to a rigid mounted rotating cylinder in flow.

III. RESULTS AND DISCUSSION

A. Results analysis and comparison

A rigid mounted rotating cylinder in flow is simulated at $Re = 10^5$, which is close to the experimental Reynolds number of Chen and Rheem (2019). The rotation rate varies from 0 to 19, the mean lift at the subcritical Reynolds number is shown in Fig. 7(a), and the variation of the mean lift of the present study is similar to the two-dimensional results of Tokumaru and Dimotakis (1993) and Chew *et al.* (1995), in whose results the mean lift increases and then remains steady with the increase in rotation rate. Compared with the previous experimental results of Chen and Rheem (2019) for different cylinders, a similar variation that increases and then remains a certain constant can be obtained and the constant is considered to be determined by the aspect ratio (the ratio of the cylinder's length and diameter). Due to the aspect ratio effect, the constant of the present study is closer to that of the cylinder with the largest aspect ratio. For the enlarged drawing of the mean lift in Fig. 8(a), the concave

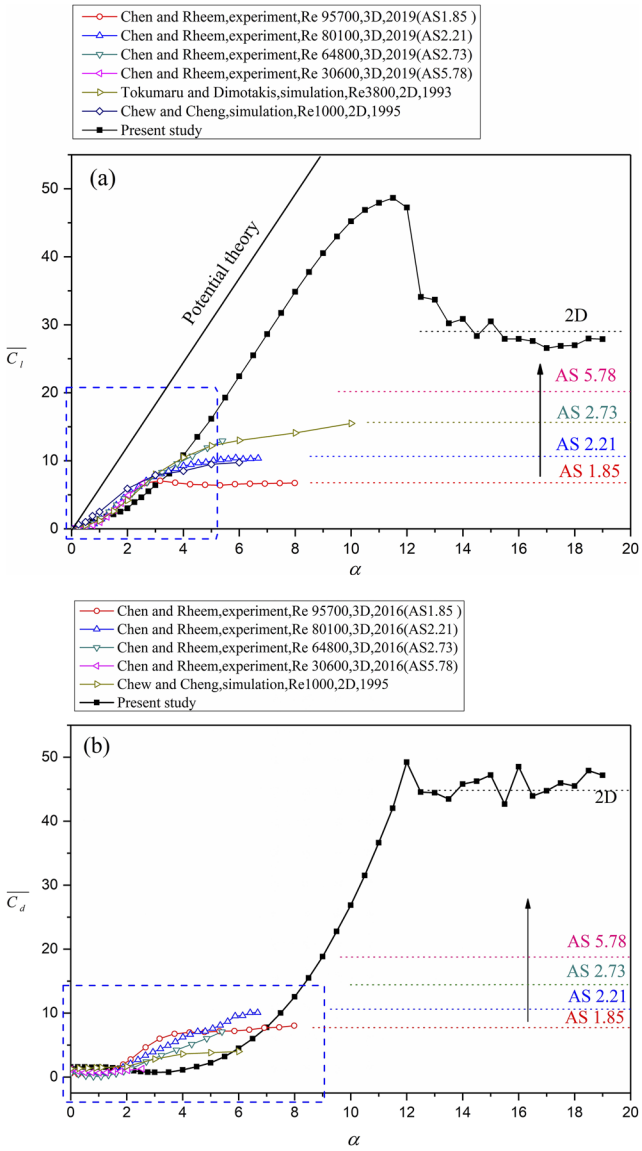

FIG. 7. (a) Mean lift coefficient, $\overline{C_l}$, and (b) mean drag coefficient, $\overline{C_d}$, vs the rotation rate, α, of the present study and previous works (2D = two-dimensional; 3D = three-dimensional).

increasing shape of the present study is similar to that of the work of Chen and Rheem (2019); a little difference is that the concave increasing shape of the present study has been postponed because of the aspect ratio effect.

Figure 7(b) shows a mean drag at the subcritical Reynolds number, and compared with the experimental results of Chen and Rheem (2019) for different cylinders, a similar variation can be obtained. The mean drag decreases initially, then increases, and finally remains a certain constant with the increase in rotation rate. A little difference is that the initial steady does not appear in the results of Chen and Rheem (2019). Similar to the constant of the mean lift,

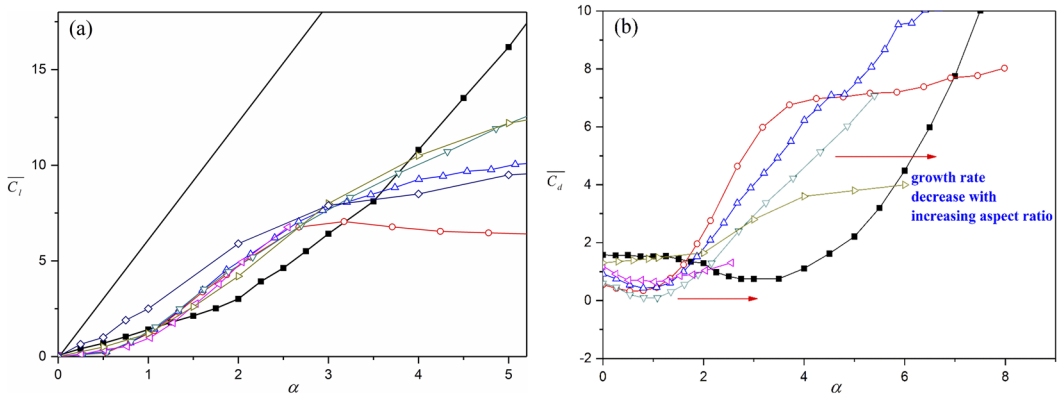

FIG. 8. (a) Enlarged drawing of the dotted box of Fig. 7(a) and (b) Enlarged drawing of the dotted box of Fig. 7(b).

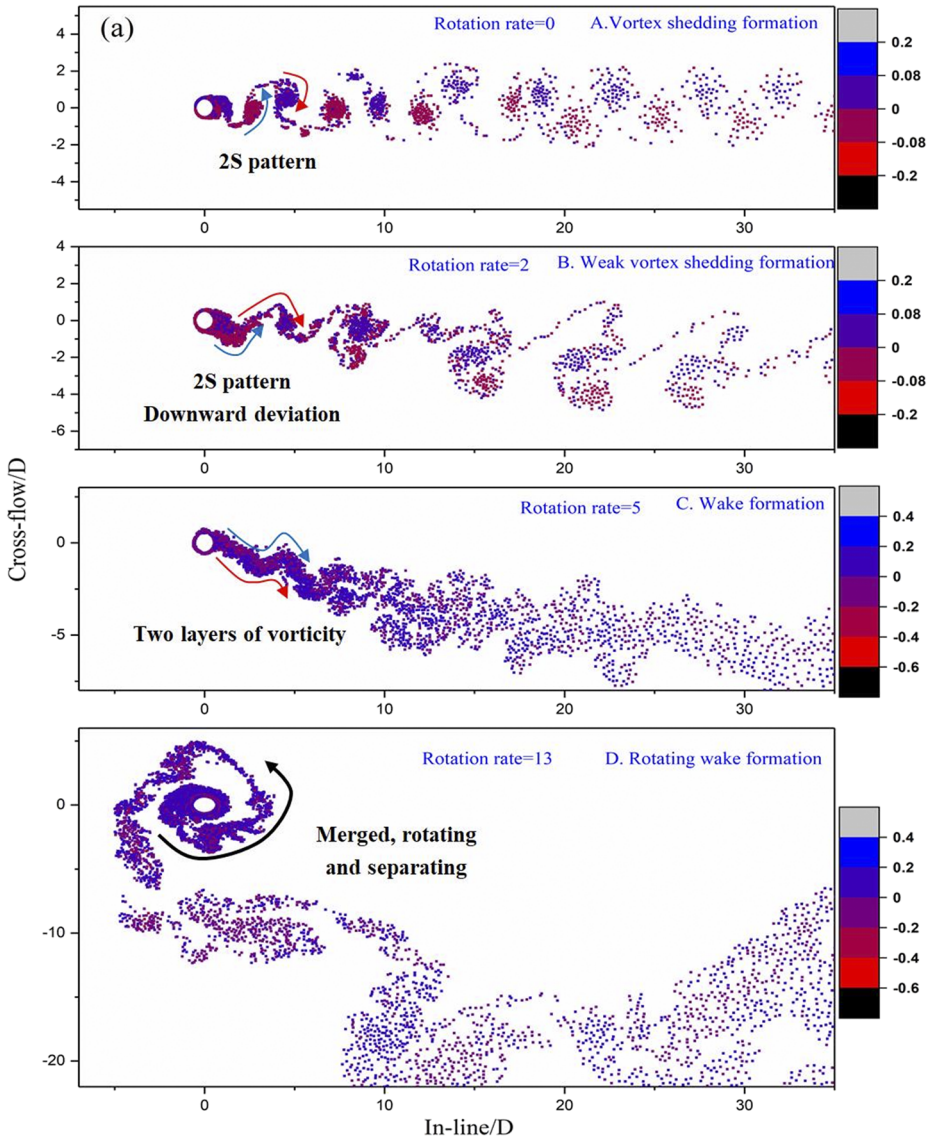

FIG. 9. (a) Wake formations at different rotation rates. (b) Time history of the hydrodynamics and (c) the corresponding frequency analysis of the lift under different rotation rates.

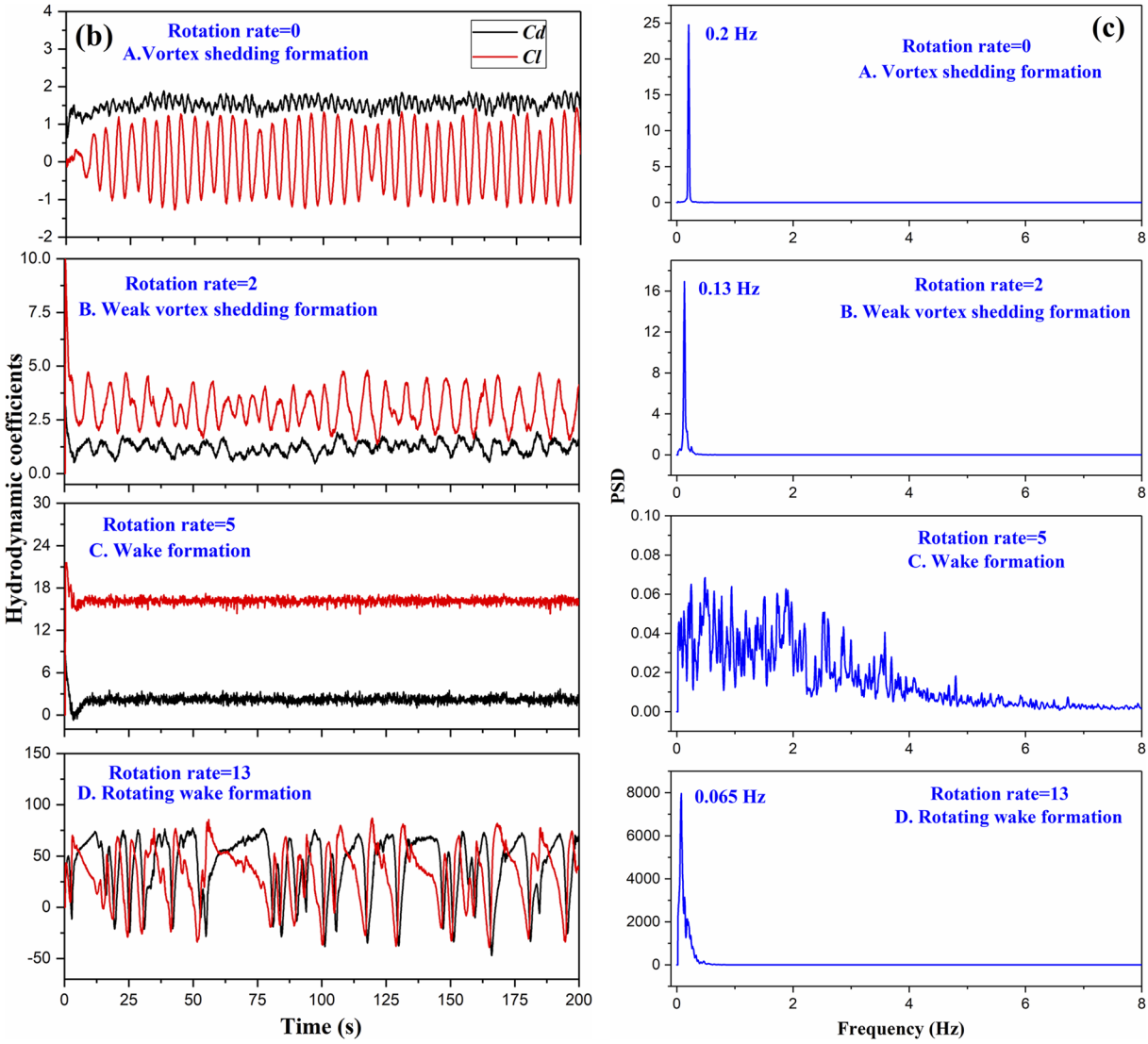

FIG. 9. *(Continued.)*

the constant of the mean drag is considered to be determined by the aspect ratio and the constant of the present study is closer to that of the cylinder with the largest aspect ratio. For the mean drag of the present study, the decrease has been postponed due to the aspect ratio effect and the growth rate of the increase decreases with increasing aspect ratio. In particular, the minimum mean drag of the present study is close to zero but without a negative value, which is in agreement with the experimental results of Chen and Rheem (2019) and differencing from the results of Stojkovic *et al.* (2002).

B. Four different wake formations

Comparisons of the mean hydrodynamics indicate that the present results are reasonable, and the present DVM is effective for a rigid mounted rotating cylinder in flow. In order to figure out the relationship between the hydrodynamics and wake formation, wake formations are analyzed and four different wake formations (vortex shedding, weak vortex shedding, wake, and rotating wake formations) are identified at rotation rates from 0 to 19. Corresponding to these different formations, the wake formation, hydrodynamics, and corresponding frequency analysis of the lift coefficient at rotation rates of 0, 2, 5, and 13 are illustrated. The characteristics of these wake formations are as follows: (A) In vortex shedding formation, the two counter rotating vortices periodically shed from the two sides of the cylinder [Fig. 9(a)], which results in the periodical hydrodynamics [Fig. 9(b)]. The wake exhibits the 2 S pattern (two single vortices per cycle). The vortex shedding frequency follows the Strouhal number of 0.2 [the most common value for vortex

shedding frequency (Blevins, 1990 and Williamson and Govardhan, 2004)] [Fig. 9(c)]. (B) In weak vortex shedding formation, the wake of the 2 S pattern and periodical hydrodynamics can still be achieved. The rotation induces an asymmetry in the strength of the positive and negative vortices. A downward deviation of the wake is induced [Fig. 9(a)]. The positive and negative vortices are a little merged, and the vortex shedding frequency is smaller than that of vortex shedding formation [Fig. 9(c)]. (C) In wake formation, the vortex shedding disappears, and in contrast to this, the wake is composed of two layers of vorticity. In particular, the negative-vorticity layer is located above the positive-vorticity layer [Fig. 9(a)]. The wake becomes steady, and no gap between the positive-vorticity

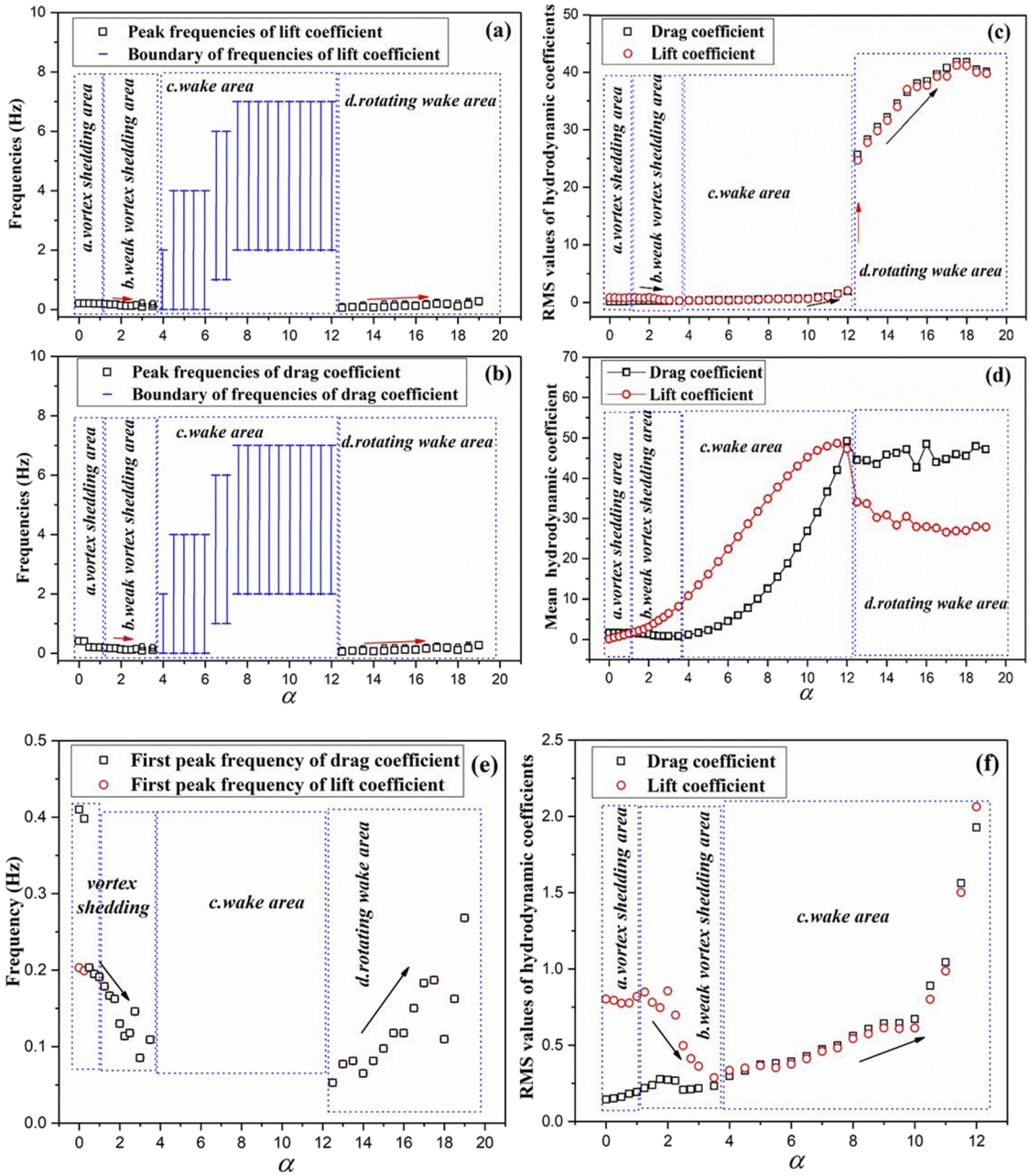

FIG. 10. Frequency of (a) lift and (b) drag coefficients, (c) rms values of hydrodynamic coefficients, and (d) mean hydrodynamics vs rotation rate. (e) First peak frequencies and (f) rms values of hydrodynamic coefficients vs rotation rate (for better describing the variation, the data in the wake area have been ignored in panel (e) and the data in the rotating wake area have been ignored in panel (f).

and negative-vorticity layers results in the steady hydrodynamics [Fig. 9(b)]. The wake formation is similar to the "D⁻ pattern" of Bourguet and Lo Jacono (2014). (D) In rotating wake formation, the positive and negative vortices completely merge together. The wake rotates around the cylinder and then separates from the cylinder [Fig. 9(a)]. The separation induces the huge fluctuation of hydrodynamics [Fig. 9(b)], and several peaks can be obtained in the frequency spectrum [Fig. 9(c)]. Actually, the present vortex shedding, weak vortex shedding, and wake formations are similar to the wake patterns of previous research studies (Mittal and Kumar, 2003 and Bourguet and Lo Jacono, 2014). Otherwise, the rotating wake formation has not been introduced in previous research studies and is a new finding in the present investigation.

Based on these four different wake formations, with the increase in rotation rate, four areas are obtained by dividing. The corresponding hydrodynamics characteristics have been illustrated in Fig. 10. (A) In the vortex shedding area at $0 \le \alpha \le 1.0$, the vortices periodically shed and the vortex shedding frequency remains steady and follows the Strouhal number of 0.2 [the most common value for vortex shedding frequency (Blevins, 1990 and Williamson and Govardhan, 2004)], which induces the steady frequency and steady rms values of the lift. The frequency of the drag is twice the frequency of the lift at a rotation rate of 0, and then, to be the same, the rotation rate of 0.5 is achieved [Fig. 10(e)] since the deflected vortices have an effect on the in-line direction, which is in agreement with the experimental results of the cylinder with a diameter of 0.319 m from the work of Chen and Rheem (2019). The deflected vortices result in the mean lift, which gradually increases, and the rms values of the drag gradually increase [Figs. 10(d) and 10(f)]. However, the mean drag remains steady in this area as the deflection of these vortices is slight. (B) In the weak vortex shedding area at $1.0 < \alpha \le 3.5$, the vortex shedding frequency decreases and the vortex shedding has been weakened, which induces decreasing of the lift frequency and rms values of the lift [Figs. 10(e) and 10(f)]. The mean lift increases with increasing rotation rate in this area. For the drag, the frequency is the same as the lift. The rms values of the drag remain steady and then become the same as those of the lift at the end of this area [Fig. 10(f)]; the mean drag decreases to a minimum as the vortex shedding frequency has been dramatically weakened. (C) In the wake area at $3.5 < \alpha \le 12$, no gap between the positive-vorticity and negative-vorticity layers results in the energy spread in a range in contrast to that at several peaks [Figs. 10(a) and 10(b)]. Similar characteristics of the lift and drag can be obtained, and the rms values of the lift and drag gradually increase. The mean lift and drag dramatically increase [Figs. 10(e) and 10(d)]. (D) In the rotating wake area at $12 < \alpha \le 19$, as the rotating wake is separated from the cylinder, the jumping of rms values of hydrodynamics can be obtained at the boundary of the wake area and rotating wake area [Fig. 10(c)]. The rotation dominates the flow field, and the effect of incoming flow has been dramatically weakened. Similar characteristics for the lift and drag can be achieved [Fig. 10(e)], and the mean hydrodynamics remains steady with the increase in rotation rate in this area [Fig. 10(d)]. As the separation of the rotating wake accelerates with the increase in rotation rate, the frequency and rms values of hydrodynamics gradually increase [Figs. 10(c) and 10(e)].

The mean resultant force coefficients (the resultant force coefficient of the mean lift and drag coefficients) and angle between the mean resultant force and the in-line direction are presented in Fig. 11; the mean resultant force increases with increasing rotation rate in vortex shedding, weak vortex shedding, and wake areas and finally remains a constant in the rotating wake area. The angle actually represents the ratio of the mean lift and drag. As the mean lift increases in the vortex shedding and weak vortex shedding areas, and mean drag decreases in the weak vortex shedding area, the angle dramatically increases in both the areas. Then, the angle gradually decreases in the wake area as the growth rate of the mean drag is larger than that of the mean lift in this area (Fig. 11). Finally, the angle remains steady in the rotating wake area, corresponding to the steady constants for the mean drag and mean lift. The variations of the mean resultant force coefficient and angle are similar to those of the cylinder with a diameter of 0.319 m from the work of Chen and Rheem (2019).

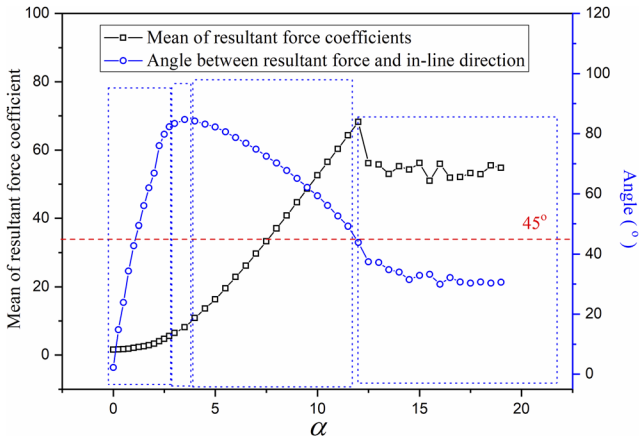

FIG. 11. Mean resultant force coefficients and angle between the mean resultant force and the in-line direction vs rotation rate.

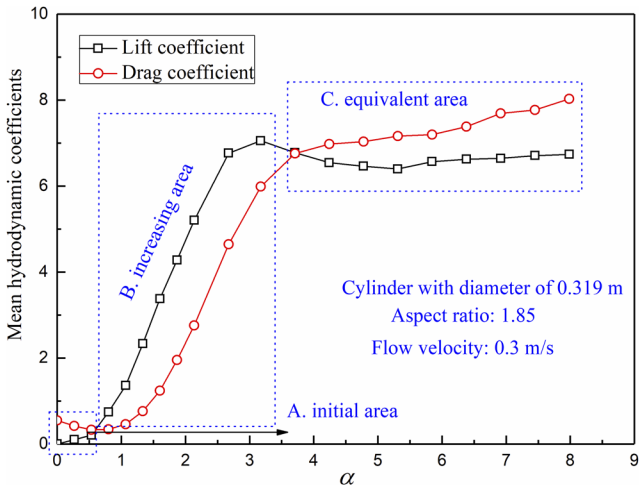

FIG. 12. Mean hydrodynamic coefficients of the cylinder with a diameter of 0.319 m vs the rotation rate of the experiment of Chen and Rheem (2019).

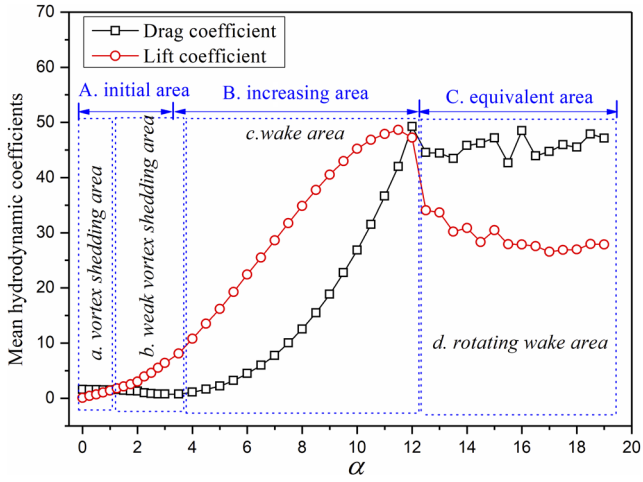

FIG. 13. Mean hydrodynamics vs rotation rate of the present study.

C. Results discussion based on two different area divisions

As shown in Fig. 12, the initial, increasing, and equivalent areas have been defined to elaborately describe the variation of the mean hydrodynamics in the experiment of Chen and Rheem (2019). Similarly, the initial, increasing, and equivalent areas can also be applied for the results of the present study, as shown in Fig. 13. The boundary of initial and increasing areas is in the weak vortex shedding area, where the vortex shedding gradually weakens and then disappears. The mean drag gradually decreases to a minimum at the boundary, the weak vortex shedding area can actually be regarded as the transitional area for vortex shedding and wake areas, and represents the end of the initial area and beginning of the increasing area. The equivalent area corresponds to the rotating wake area, where the mean hydrodynamics remains steady since the rotating wake dominates the flow, and the effect of incoming flow has been dramatically weakened. The range of initial, increasing, and equivalent areas is considered to be determined by the aspect ratio (Chen and Rheem, 2019), which explains that the range of these areas of the experiment of Chen and Rheem (2019) is narrower than that of the present study.

D. Discussion of vortex shedding and the Strouhal number

Vortex shedding of a rotating cylinder in flow has been investigated by a few researchers, and the critical α for the vortex shedding disappearance of their results is a little different (Diaz *et al.*, 1983; Coutanceau and Menard, 1985; Chew *et al.*, 1995; Degani *et al.*, 1998; Mittal and Kumar, 2003; and Chen and Rheem, 2019). In order to discuss the vortex shedding phenomenon in detail, the wake formations at rotation rates of 0, 1, 1.75, and 2.5 are shown in Fig. 14(a).

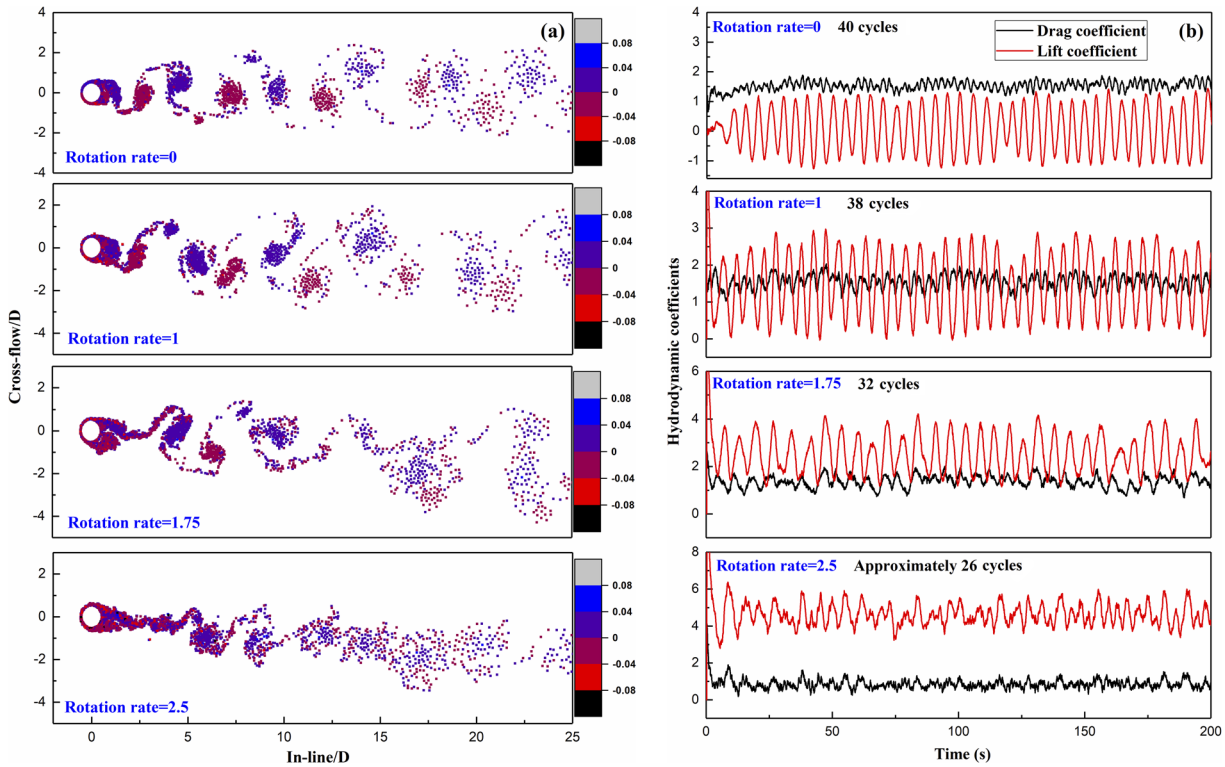

FIG. 14. (a) Wake formation at different rotation rates at a certain time and (b) time history of hydrodynamic coefficients at corresponding rotation rates.

At $\alpha = 0$, five pairs of symmetrical vortices can be obtained in the calculation area and the positive and negative vortices can be distinguished apparently. As the rotation rate increased to 1, five pairs of vortices can still be viewed, which are similar to those at $\alpha = 0$, but slightly inclined to the rotating direction. Once the rotation rate is increased to 1.75, only four pairs of vortices can be observed in the calculation area, and the positive and negative vortices cannot be distinguished apparently as that at $\alpha = 0$ and $\alpha = 1$. When the rotation rate increased to 2.5, only two pairs of vortices near the rotating cylinder can be achieved since the vortices far from the rotating cylinder merge together and become a steady wake. Actually, it is a little difficult to obtain an exact critical α for the disappearance of vortex shedding; Degani *et al.* (1998) suggested a critical value equal to 1.91 based on their calculation results. Coutanceau and Menard (1985) discovered that the critical rotation rate is approximately $\alpha \approx 2.0$. However, unlike those findings, as shown in Fig. 10(e), the critical α of the present study is approximately 3.5, which is close to the results of Diaz *et al.* (1983), Chew *et al.* (1995), and Chen and Rheem (2019) at subcritical Reynolds numbers, which suggest that the critical α is at $\alpha \approx 3.0$.

Corresponding to the wake formations, the time histories of hydrodynamics at these four rotation rates are presented in Fig. 14(b). At $\alpha = 0$, the periodical phenomenon of the hydrodynamics can be observed, 40 cycles of lift exist in $t = 200$ s, and the frequency of the drag is approximately two times that of the lift. As the rotation rate increased to 1.0, the mean lift increases and 38 cycles of lift can be observed. However, unlike that at $\alpha = 0$, the frequency of the drag is almost the same as that of the lift. As the rotation rate increased to 1.75 and 2.5, the mean lift gradually increases and the cycles of the lift decrease to approximately 32 at $\alpha = 1.75$ and 26 at $\alpha = 2.5$, respectively. The decrease in the cycles of the lift corresponds to the decreasing number of vortices in Fig. 14(a).

One intriguing question concerning vortex shedding is the variation of the Strouhal number, *St*. With increasing rotation rate, the Strouhal number of the present study and previous works is shown in Fig. 15. The decrease in the Strouhal number is insisted by Kang *et al.* (1999), Mittal and Kumar (2003), and Kumar *et al.* (2011b). For the present study, the decrease is severe than that of the results of those researchers at low Reynolds numbers and close to that of Chen and Rheem (2019) at subcritical Reynolds numbers. Similar to the results of Chen and Rheem (2019), the variation of the Strouhal number of the present study remains steady initially, then decreases, and finally disappears.

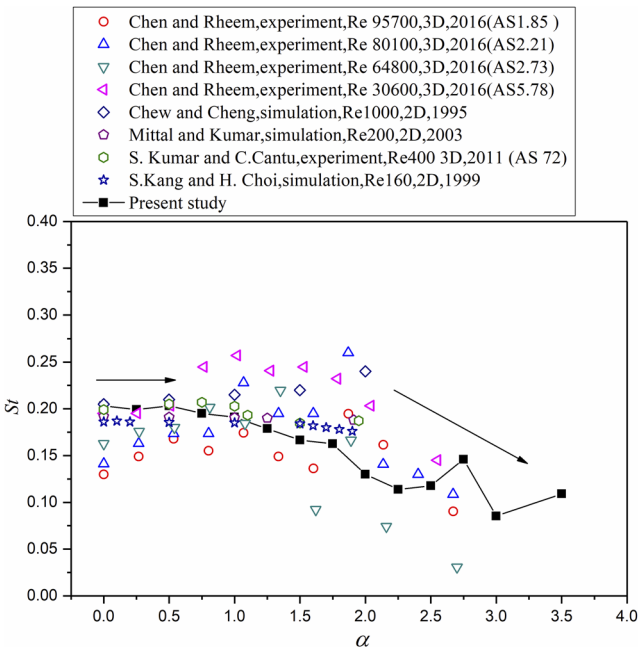

FIG. 15. Strouhal number, *St*, vs rotation rate, α, of the present study and previous works (2D = two-dimensional and 3D = three-dimensional).

IV. CONCLUSIONS

A rotating cylinder placed in flow is investigated by using a two-dimensional discrete vortex simulation method at $0 < \alpha \leq 19$. Based on the no-slip condition, the simplified Navier–Stokes equation is solved by using the relationship between the surface pressure gradient and generated surface vortex strength. The results are discussed, and the principle findings of this work are summarized.

First, the mean hydrodynamics has been illustrated, and the mean lift of the present study increases and then seems to be steady at a certain constant with the increasing rotation rate. Combined with the previous works, the constant is considered to be determined by the aspect ratio, and the constant of the present study is closer to that of the cylinder with the largest aspect ratio. The mean drag of the present study decreases initially, then increases, and finally remains a certain constant with the increase in rotation rate. Similar to the constant of the mean lift, the constant of the mean drag is considered to be determined by the aspect ratio, and the constant of the present study is closer to that of the cylinder with the largest aspect ratio. The initial decrease in the mean drag has been postponed due to the aspect ratio effect, and the growth rate of the increase at the increasing stage decreases with increasing aspect ratio. In particular, the minimum mean drag of the present study is close to zero, but without negative values.

Next, the relationship between the hydrodynamics and the wake formation has been discussed. The wake has been dramatically affected by the imposed rotation. The vortex shedding, weak vortex shedding, wake, and rotating wake formations have been identified and illustrated. Under vortex shedding and weak vortex shedding formations, periodical hydrodynamics is induced. Under wake formation, no gap between the positive-vorticity and negative-vorticity layers results in the steady hydrodynamics. The separation of the rotating wake induces huge fluctuations of the hydrodynamics under rotating wake formation. Corresponding to the different characteristics, the vortex shedding, weak vortex shedding, wake, and rotating wake areas are identified and the variation of hydrodynamics in these areas is illustrated.

Then, the initial, increasing, and equivalent areas have been applied for the mean hydrodynamics of the present study, combined with vortex shedding, weak vortex shedding, wake, and rotating wake areas from wake formations. The weak vortex shedding area

(the transitional area of vortex shedding and wake areas) represents the end of the initial area and beginning of the increasing area, where vortex shedding gradually weakens and then disappears, inducing a mean drag that gradually decreases to a minimum. The rotating wake area corresponds to the equivalent area, where rotation dominates the flow field and the effect of incoming flow has been dramatically weakened, maintaining steady mean hydrodynamics.

Finally, the disappearance of vortex shedding and the Strouhal number are discussed in detail, the disappearance of vortex shedding at $\alpha \approx 3.5$ is concluded in the present study, and the Strouhal number (vortex shedding frequency) remains steady initially and then decreases with the increasing rotation rate.

ACKNOWLEDGMENTS

This research was funded by the National Natural Science Foundation of China (Grant No. 51979215), Scientific Research Funding for the Doctors of Wuhan University of Technology (Grant No. WUT: 40120268), the Fundamental Research Funds for the Central Universities (Grant No. WUT: 2019IVA059), and Australia Research Council DECRA (Grant No. DE190100931).

The authors declare that there are no conflicts of interest.

DATA AVAILABILITY

The data that support the findings of this study are available from the corresponding author upon reasonable request.

REFERENCES

Al-Jamal, H. and Dalton, C., "Vortex induced vibrations using large eddy simulation at a moderate Reynolds number," J. Fluids Struct. **19**(1), 73–92 (2004).

Bearman, P. W., "Vortex shedding from oscillating bluff bodies," Annu. Rev. Fluid Mech. **16**(1), 195–222 (1984).

Blevins, R. D., *Flow-Induced Vibration* (Krieger Publishing Company, FL, 1990).

Bourguet, R. and Lo Jacono, D., "Flow-induced vibrations of a rotating cylinder," J. Fluid Mech. **740**(4), 342–380 (2014).

Chen, W. and Rheem, C.-K., "Experimental investigation of rotating cylinders in flow," J. Marine Sci. Technol. **24**, 111–122 (2019).

Chew, Y. T. *et al.*, "A numerical study of flow past a rotating circular cylinder using a hybrid vortex scheme," J. Fluid Mech. **299**(299), 35–71 (1995).

Coutanceau, M. and Ménard, C., "Influence of rotation on the near-wake development behind an impulsively started circular cylinder," J. Fluid Mech. **158**, 399–446 (1985).

Degani, A. *et al.*, "Unsteady separation past moving surfaces," J. Fluid Mech. **375**, 1–38 (1998).

Diaz, F. *et al.*, "Vortex shedding from a spinning cylinder," Phys. Fluids **26**(12), 3454–3460 (1983).

Du, L. and Dalton, C., "LES calculation for uniform flow past a rotationally oscillating cylinder," J. Fluids Struct. **42**, 40–54 (2013).

Evangelinos, C. *et al.*, "DNS-derived force distribution on flexible cylinders subject to vortex-induced vibration," J. Fluids Struct. **14**(3), 429–440 (2000).

Fujisawa, N. *et al.*, "Feedback control of vortex shedding from a circular cylinder by rotational oscillations," J. Fluid Struct. **15**(1), 23–37 (1991).

Hadžiabdić, M. *et al.*, "Heat transfer in flow around a rotary oscillating cylinder at a high subcritical Reynolds number: A computational study," Int. J. Heat Fluid Flow **79**, 108441 (2019).

HonoréWalther, J. and Larsen, A., "Two dimensional discrete vortex method for application to bluff body aerodynamics," J. Wind Eng. Ind. Aerodyn. **67-68**(97), 183–193 (1997).

Kang, S. *et al.*, "Laminar flow past a rotating circular cylinder," Phys. Fluids **11**(11), 3312–3321 (1999).

Karabelas, S. J. *et al.*, "High Reynolds number turbulent flow past a rotating cylinder," Appl. Math. Modell. **36**(1), 379–398 (2012).

Kimura, T. and Tsutahara, M., "Flows about a rotating circular cylinder by the discrete-vortex method," AIAA J. **25**(1), 182–184 (1987).

Korpus, R. *et al.*, "Prediction of viscous forces on oscillating cylinders by Reynolds-averaged navier-stokes solver," in *Tenth International Offshore and Polar Engineering Conference* (International Society of Offshore and Polar Engineers, 2000).

Koumoutsakos, P. and Leonard, A., "High-resolution simulations of the flow around an impulsively started cylinder using vortex method," J. Fluid Mech. **296**(296), 1–38 (1995).

Kumar, S. *et al.*, "Flow past a rotating cylinder at low and high rotation rates," J. Fluids Eng. **133**(4), 041201 (2011a).

Kumar, S. *et al.*, "Flow past two rotating cylinders," Phys. Fluids **23**(1), 014102 (2011b).

Lamb, H., *Hydrodynamics* (Cambridge University Press, 1993).

Lewis, R. I., *Vortex Element Methods for Fluid Dynamic Analysis of Engineering Systems* (Cambridge University Press, 2005).

Mittal, S., "Three-dimensional instabilities in flow past a rotating cylinder," J. Appl. Mech. **71**(1), 89–95 (2004).

Mittal, S. and Kumar, B., "Flow past a rotating cylinder," J. Fluid Mech. **476**, 303–334 (2003).

Modi, V. J., "Moving surface boundary-layer control: A review," J. Fluids Struct. **11**(6), 627–663 (1997).

Munir, A. *et al.*, "Three-dimensional numerical investigation of vortex-induced vibration of a rotating circular cylinder in uniform flow," Phys. Fluids **30**(5), 053602 (2018).

Mustto, A. *et al.*, *Discrete Vortex Method Simulation of the Flow Around a Circular Cylinder with and without Rotation* (American Institute of Aeronautics and Astronautics, 1998).

Palkin, E. *et al.*, "Control of flow around a cylinder by rotary oscillations at a high subcritical Reynolds number," J. Fluid Mech. **855**, 236–266 (2018).

Prandtl, L., "The Magnus effect and windpowered ships," Naturwissenschaften **13**(6), 93–108 (1925).

Rao, A. *et al.*, "Three-dimensionality in the wake of a rotating cylinder in a uniform flow," J. Fluid Mech. **717**(5), 1–29 (2013).

Rao, A. *et al.*, "A review of rotating cylinder wake transitions," J. Fluids Struct. **53**, 2–14 (2015).

Schlichting, H. and Gersten, K., *Boundary-Layer Theory* (Springer, 2016).

Schulmeister, J. C. *et al.*, "Flow control with rotating cylinders," J. Fluid Mech. **825**, 743–763 (2017).

Shiels, D. and Leonard, A., "Investigation of a drag reduction on a circular cylinder in rotary oscillation," J. Fluid Mech. **431**, 297–322 (2001).

Stojkovic, D. *et al.*, "Effect of high rotation rates on the laminar flow around a circular cylinder," Phys. Fluids **14**(9), 3160–3178 (2002).

Sun, J. *et al.*, "Experimental study on the flow past a rotating cylinder with PIV," J. Exp. Fluid Mech. **30**, 81–90 (2016).

Tokumaru, P. T. and Dimotakis, P. E., "The lift of a cylinder executing rotary motions in a uniform flow," J. Fluid Mech. **255**(255), 1–10 (1993).

Williamson, C. H. K. and Govardhan, R., "Vortex-induced vibrations," Annu. Rev. Fluid Mech. **36**, 413–455 (2004).

Williamson, C. H. K. and Roshko, A., "Vortex formation in the wake of an oscillating cylinder," J. Fluids Struct. **2**(4), 355–381 (1988).

Yamamoto, C. T. *et al.*, "Numerical simulations of vortex-induced vibration on flexible cylinders," J. Fluids Struct. **19**(4), 467–489 (2004).